Pergamon

Int. J. Solids Structures Vol. 32, No. 17/18, pp. 2725–2743, 1995

0020-7683/95 $9.50 + .00

0020-7683(94)00298-3

OSCILLATORY FRACTURE IN POLYMERIC MATERIALS

T. W. WEBB† and E. C. AIFANTIS‡
Center for Mechanics of Materials and Instabilities, Michigan Technological University, Houghton, MI 49931, U.S.A.

(*Received* 3 *February* 1994)

Abstract—A "stick–slip" fracture model based on an "inertia-dependent" modified equation of motion for the crack tip and a "non-monotonic" fracture toughness–velocity curve is presented and analyzed with the aid of techniques commonly used in non-linear dynamics. As a result of an analysis for constant applied extension rate fracture tests, macroscopic stick–slip fracture oscillations (with crack jump increments larger than the length of the "fracture process zone") are shown to be self-oscillations and described by a limit cycle in the energy release rate–crack tip velocity plane. Numerical results are presented and compared with experimental stick–slip fracture observations.

1. INTRODUCTION

The phenomenon of "stick–slip" (or "arrest–fast propagation") fracture is commonly observed in standard fracture tests of polymers and peel tests of polymeric adhesives. Stick–slip fracture or peeling can occur on both microscopic and macroscopic scales and is characterized by an oscillatory crack tip velocity and crack growth jumps. Stick–slip fracture on a microscopic scale is the case where the size of the crack jump increments is comparable with the size of the fracture process zone and the crack tip velocity oscillations and their effects are usually "averaged" out in experiments. Examples of such behavior are observed in dynamic fracture tests where crack tip velocity oscillations result in a periodic structure on the fracture surface (Fineberg *et al.*, 1991, 1992). Stick–slip fracture on a macroscopic scale is the case where the size of the crack jump increments is much larger than the size of the fracture process zone and cannot be easily "averaged" out in experiments. For example, under constant applied extension rate loading conditions, macroscopic stick–slip fracture is characterized by a sawtooth load versus time profile where the drop in load corresponds to initiation and fast propagation of macroscopic crack growth. Examples of such behavior in fracture tests under constant applied extension rates are observed in crack growth of polymethylmethacrylate (PMMA) (Atkins *et al.*, 1975; Hakeem and Phillips, 1979; Ravi-Chandar and Balzano, 1988), thermosetting polyesters (Leevers, 1986) and epoxy resins (Selby and Miller, 1975; Kobayashi and Dally, 1977; Yamini and Young, 1977; Phillips *et al.*, 1978; Kinloch and Williams, 1980; Scott *et al.*, 1980), tearing of rubber (Greensmith and Thomas, 1955; Isherwood and Williams, 1978), as well as in peeling of polymeric adhesives (Gardon, 1963; Aubrey *et al.*, 1969; Aubrey, 1978; Maugis and Barquins, 1987; Kim and Kim, 1988; Kinloch and Yuen, 1989). In addition, periodic transverse crack arrest marks and/or oscillatory crack tip velocities were observed in constant extension rate fracture tests of PMMA (Hakeem and Phillips, 1979; Carlsson *et al.*, 1972; Takahashi, 1987) and epoxy resins (Young and Beaumont, 1976; Yamini and Young, 1979; Scott *et al.*, 1980; Takahashi, 1987), as well as in peeling of polymeric adhesives (Maugis and Barquins, 1987; Kim and Kim, 1988).

Typically, stick–slip fracture on a microscopic scale may be interpreted on the basis of a discrete fracture process zone model. The fracture process zone is defined as a small region ahead of the crack tip where material degradation and local fracture processes occur. It is assumed that after some waiting time the material in the fracture process zone ruptures,

† NRC Research Associate, Naval Research Laboratory, Washington, D.C. 20375, U.S.A.
‡ Also at: Laboratory of Mechanics and Materials, Aristotle University of Thessaloniki, Thessaloniki 54006, Greece.

the crack advances the length of the process zone rapidly and arrests. The process repeats itself after some waiting time giving rise to discontinuous crack growth on a microscopic scale. Stick–slip fracture on a macroscopic scale cannot be interpreted using the fracture process zone model since the size of the crack jump increment is significantly larger than the process zone length. In this case, stick–slip fracture has been associated with the negative slope region(s) of a macroscopic non-monotonic (non-convex) "fracture toughness" versus "velocity" curve. For example, stick–slip fracture occurs when the applied extension rate and load are such that they tend to impose a crack tip velocity within the negative slope region of the non-monotonic fracture toughness versus velocity curve. Roughly speaking, steady continuous crack propagation cannot be observed in this unstable region where the resistance to crack growth decreases for an incremental increase of the crack tip velocity. Instead, the crack tip velocity oscillates by following a limit cycle in the crack tip energy release rate–velocity plane determined by the elastic behavior of the fracture specimen (and testing machine) and the crack tip velocity dependence of the fracture toughness.

Several investigators have intuitively proposed that macroscopic stick–slip fracture oscillations are manifested as closed curves or cycles in the energy release rate (or stress intensity factor)–velocity plane (Ripling *et al.*, 1964; Irwin, 1964; Irwin and Paris, 1971; Williams *et al.*, 1968; Williams, 1984; Kramer and Hart, 1984; Maugis, 1985). In particular, Barenblatt and Salganik (1963) went even further and proposed a specific model interpreting macroscopic stick–slip fracture as a self-oscillatory process. More recently, Maugis and Barquins (1987) and Webb and Aifantis (1989) viewed stick–slip peeling periodicities as self-oscillations. In the present paper this point of view is generalized and applied to interpret stick–slip fracture and the corresponding oscillations observed in polymeric materials.

Non-monotonic fracture toughness versus velocity curves and related theoretical models are reviewed in Section 2. In Section 3 a mathematical model is presented for macroscopic stick–slip fracture by incorporating an "inertia" term into the usual equation of motion for the crack tip. Finally, in Section 4 numerical results are presented for macroscopic stick–slip fracture and compared with some experimental measurements on epoxy resins that were available in the literature.

2. NON-MONOTONIC FRACTURE TOUGHNESS–VELOCITY CURVES

Although stick–slip fracture is a widely observed phenomenon, non-monotonic fracture toughness–velocity curves over a wide range of crack tip velocities have been measured only for a few materials, such as PMMA (Johnson and Radon, 1972; Green and Pratt, 1974; Atkins *et al.*, 1975; Broutman and Kobayashi, 1972), thermosetting polyesters (Leevers, 1986), rubber (Greensmith and Thomas, 1955), as well as during peeling of adherands bonded to substrates with polymeric adhesives (Aubrey *et al.*, 1969; Aubrey, 1978; Maugis and Barquins, 1987; Aubrey and Sherriff, 1980; Kinloch and Yuen, 1989). In these cases, a typically "measured" non-monotonic fracture toughness–velocity curve with two stable branches (low and high velocity) separated by an unstable stick–slip region is shown schematically in Fig. 1(a). In other situations three stable branches are observed with two unstable stick–slip fracture regions (Aubrey, 1978; Broutman and Kobayashi, 1972; Kinloch and Yuen, 1989). In the case of epoxy resin polymers (Yamini and Young, 1977, 1979; Phillips *et al.*, 1978; Scott *et al.*, 1980) there is no stable low velocity branch and the non-monotonic fracture toughness–velocity curve is as shown schematically in Fig. 1(b). This type of curve is typical for materials where the energy release rate required for crack initiation is higher than that required for crack propagation. It is important to point out that the unstable "negative slope" region is not actually measured. Instead, it is generally defined by the crack tip energy release rate corresponding to the maximum or average load of the characteristic sawtooth load profile for an average crack tip velocity rather than the actual velocity. In this connection, it is emphasized that even though it was assumed that the fracture toughness is a material property, its value cannot be measured directly. Instead, it is inferred from measurements pertaining to the critical values of the energy release rate or stress intensity factor necessary for crack propagation.

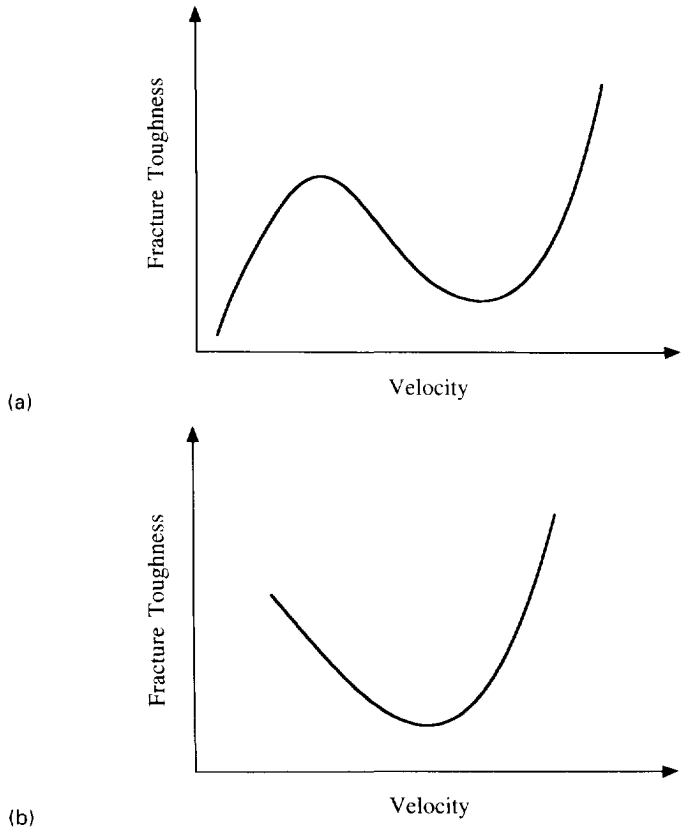

Fig. 1. Schematics of typical non-monotonic fracture toughness–velocity curves.

Several possible mechanisms have been proposed to explain qualitatively the existence of an unstable negative slope region in the fracture toughness–velocity curve in these materials. Greensmith and Thomas (1955) observed in rubber the formation of a strengthening (toughening) structure at the crack tip due to crystallization. It was reasoned that the size of the structure and the toughening effect would decrease with increasing crack tip velocity giving rise to the negative slope region. Williams (1972) proposed that the transition in the fracture toughness–velocity curve of PMMA from a positive slope to a negative slope was due to a transition from isothermal to adiabatic conditions at the crack tip. The reduction in the fracture toughness with increasing velocity was associated with the local thermal softening near the crack tip attributed to the heat generated by the viscous fracture processes, which was assumed to increase with increasing velocity. Johnson and Radon (1972) identified fracture mode transitions in PMMA with molecular relaxations and changes in the internal friction (viscosity) of the material, possibly in connection with the onset of adiabatic conditions at the crack tip over a range of velocities. Maugis (1985) associated viscoelastic losses near a moving crack tip with the fracture toughness in polymers. It was suggested that during the loading and unloading cycle, which occurs as the crack tip approaches and passes a material point, viscoelastic losses occur as a result of hysteresis. The frequency of this cycle was assumed to be proportional to the crack tip velocity and the "viscoelastic" losses were assumed to be proportional to the imaginary part of the complex Young's modulus (loss modulus). Therefore, it was proposed that a negative slope region in the fracture toughness–velocity curve may effectively represent the observed decreases of the loss modulus in polymers with increasing cyclic frequency.

It is interesting to note that several crack tip analyses already exist for steady state crack propagation which "predict" negative slope branches in their "fracture toughness" versus "velocity" curves. These negative slope branches obviously represent unstable crack growth and contain states that cannot be attained by the material for steady crack velocities. It follows that these models breakdown in these regimes where stable "steady" crack

propagation is not possible but, instead, unstable stick–slip fracture occurs. Hart (1980, 1983) and Kramer and Hart (1984) developed a model for quasi-static, steady state crack growth in ductile materials. The model is based on the assumption that the crack tip stress state is characterized by an inverse square root singularity and a local stress intensity factor and makes use of the self-stresses of the plastic (or craze) zone represented by a continuous distribution of dislocations. The self-stresses consist of singular and non-singular terms with the singular terms being characterized by a plastic stress intensity (which is added to the usual elastic stress intensity factor to obtain the total local stress intensity factor). The plastic stress intensity factor acts to screen or shield the crack tip and is assumed to be a function of the crack tip velocity and local stress intensity factor since the plasticity (or inelasticity) in the plastic (or craze) zone is strain rate sensitive and dependent on the level of stress at the crack tip. By assuming various brittle crack growth laws in terms of the local crack tip stress intensity factor, non-monotonic fracture toughness–velocity curves like those in Fig. 1(a) (Hart, 1980) and in Fig 1(b) (Kramer and Hart, 1984) were determined. Thus, the model suggests that at high velocities a breakaway phenomenon may occur in which the crack outruns the ability of the plastic (or craze) zone to shield the crack tip.

Similar results were obtained in the analysis of quasi-static, steady state crack growth under small scale yielding conditions in an elastic–viscous material (Hui and Riedel, 1981; Hui, 1983; Riedel, 1990). The asymptotic stress and strain fields for a quasi-statically growing crack in an elastic–viscous material were derived by Hui and Reidel (1981). In a power-law creep material it was shown that for a creep coefficient $n < 3$ the asymptotic stress and strain fields are given by the usual inverse square-root singularity, which was also assumed by Hart (1980) in his analysis. For $n > 3$ a different singularity (known as the HR singularity) less than the inverse square-root singularity was determined [i.e. $\varepsilon \sim (v/r)^{1/(n-1)}$, where v is the crack tip velocity and r denotes the radial distance from the crack tip]. It was assumed that the remote boundary condition ($r \to \infty$) for steady state crack growth under small-scale yielding conditions is given by the elastic stress field and the near crack tip fields are given by the HR fields (i.e. $n > 3$). The crack was assumed to advance when the effective strain at a critical distance from the crack tip obtains a critical value. The resulting non-monotonic fracture toughness–velocity curve is like that in Fig. 1(b). The unstable branch corresponds to the case where the strain is primarily determined by the HR field. The HR field is mostly dominant (and the size of the creep zone is maximum) at the point of minimum fracture toughness and decreases on the stable branch for increasing stress intensity factor until the elastic strain dominates the creep strain.

Non-monotonic fracture toughness–velocity curves are also determined in dynamic fracture analyses for elastic–viscoplastic materials (Freund and Hutchinson, 1985; Freund *et al.*, 1986; Mataga *et al.*, 1987). Steady state crack growth and small-scale yielding conditions are assumed and in the analyses it is envisioned that the plastic zone travels with the moving crack tip leaving behind a plastic wake. It is assumed that the material very near the crack tip and deep within the plastic zone is elastic-like since it experiences very high strain rates as the crack propagates. Thus, the stress state at the crack tip is assumed to be elastic and identical to the remote elastic stress state except that it is characterized by a local stress intensity factor (or local energy release rate), which differs from the remote or applied stress intensity factor (or applied energy release rate) through a shielding term associated with the energy dissipated in the plastic wake. The stress state in the plastic zone is assumed and the plastic strain rate in the plastic zone is determined from the assumed plastic flow rule. The plastic dissipation or shielding term is determined from the crack tip analyses and the hypothesis that crack growth occurs when the local energy release rate reaches a critical value (assumed to be a material constant). It then turns out that the applied energy release rate required to move a crack at velocity v (i.e. fracture toughness–velocity curve) is as shown in Fig. 1(b). At low velocities there is sufficient time for plastic deformation to occur and a large applied energy release rate is required to move the crack. This effect decreases with increasing velocity until the material inertia plays a role. The inertial resistance of the material causes the energy release rate required to propagate the crack to increase with increasing velocity.

Popelar (1990) expanded the usual cleavage fracture models to include a ductile fracture mode. It was demonstrated in his analysis that at low crack tip velocities the elastic region near the crack tip becomes very small compared with the size of the plastic zone. In this case, ductile fracture occurs and crack growth is assumed to occur when the effective plastic strain reaches a critical value at a critical distance ahead of the crack tip. The result is that the fracture toughness–velocity curve has a stable positive slope branch at low velocities and since the cleavage fracture is assumed to occur at higher velocities then the fracture toughness–velocity curve would be as shown in Fig. 1(a)

Freund and Lee (1990) also examined fracture mode transitions in dynamic crack growth. The plastic zone was approximated as a one-dimensional cohesive zone ahead of the crack tip and the cohesive stresses were assumed to depend on the local opening rate. In their analysis crack growth was permitted to occur in either a cleavage (critical stress) or ductile (critical crack tip opening displacement) mode depending on which of the two competing modes prevails, and fracture toughness–velocity curves as in Fig. 1(a) were also predicted.

The qualitative behavior of the non-monotonic fracture toughness–velocity curves is successfully captured using the crack tip analyses and models outlined above. While this fact in itself demonstrates the appropriateness and physical reasonableness of these models, there are certain serious difficulties which arise, especially when the implications of the negative slope regime are not considered properly. For example, in the dynamic analyses (Freund and Hutchinson, 1985; Freund *et al.*, 1986; Mataga *et al.*, 1987) the minimum in the fracture toughness–velocity curve occurs at approximately half the Rayleigh wave speed C_R and the fracture toughness approaches infinity at C_R. Experimentally, dynamic crack growth rates seldom exceed $0.3C_R$–$0.4C_R$. This difficulty may be attributed to the occurrence of crack tip velocity oscillations observed in dynamic crack growth experiments (Fineberg *et al.*, 1991, 1992). In this case the fracture process zone size is not constant and possibly the crack propagation process can no longer be reasonably approximated as steady state in these analyses. (Note, in this connection, that the aforementioned negative slope region cannot be physically envisioned as corresponding to steady state crack propagation.) Moreover, these crack tip analyses and models do not consider the experimentally observed loading rate dependence of the fracture toughness at initiation. Specifically, it is observed in epoxy resins (Yamini and Young, 1977, 1979; Phillips *et al.*, 1978; Scott *et al.*, 1980) that the crack initiation toughness decreases with increasing applied extension or loading rates, a fact suggesting that the crack growth history can no longer be simply described by a velocity-dependent fracture toughness.

Some of the above difficulties are overcome in the model outlined in the next section where the assumptions of a loading curve, non-convexity of the fracture toughness–velocity curve and crack tip inertia are adopted. Within the resulting framework, one can then interpret the oscillations observed during stick–slip fracture and account for the corresponding effects of pre-macroscopic crack initiation processes, such as, crack tip blunting and microcrack/void development, which manifest themselves in the appearance of the upper (initiation) and lower (arrest) stress intensity factors.

3. STICK SLIP FRACTURE MODEL

In this section the basic equations for stick–slip fracture are derived. The usual equation of motion for the crack tip is modified by introducing an additional term which includes the crack tip acceleration in order to capture the non-steady crack growth behavior that occurs during stick–slip fracture. This additional term is referred to as the crack tip inertia and its coefficient is referred to as the "effective" mass of the crack. The governing equations for macroscopic stick–slip fracture are derived from an analysis of the constant extension rate fracture test. For different crack geometries and specimen configurations, these equations may be approximately cast into a common mathematical form and then examined using techniques from non-linear dynamics. A preliminary discussion of this approach was included in reviews by Aifantis (1990, 1991, 1992) and its mathematical analysis parallels the one presented by Webb and Aifantis (1989) for peeling.

Roughly speaking, stick–slip fracture involves both a slow, subcritical or apparent crack growth stage ("stick') and a fast or dynamic crack growth stage ("slip"). Thus, in general, during stick–slip fracture the concepts of dynamic fracture mechanics may be used. A simple result from rather involved analyses (Freund, 1990) is that the dynamic energy release rate G_d can be expressed as the product of a universal function $g(v) = 1 - v/C_R$ (referred to as the material inertial shielding term) and the "static" equilibrium energy release rate G, that is,

$$G_d = g(v)G. \tag{1}$$

It follows that the dynamic energy release rate G_d depends only on the crack length a through G and the instantaneous crack tip velocity v through the function $g(v)$; but is independent of the history of crack tip motion (e.g. crack tip acceleration). This is because higher order terms in the crack tip stress and strain fields, which depend on the crack tip acceleration, drop out in the "asymptotic" determination of the near tip energy release rate G_d (Freund, 1990; Freund and Rosakis, 1992).

The equation of motion for a propagating crack may be written in the general form (Freund, 1990)

$$G_d(a,\ v;\ \text{loading history, geometry, moduli}, \dots) = \gamma, \tag{2}$$

where γ is the fracture toughness or specific fracture energy. The fracture toughness represents the resistance of the material to crack growth. It is usually assumed to depend on the crack tip velocity v. However, inherent in this assumption is the hypothesis of steady state or "asymptomatically" steady state crack growth. There is no provision in eqn (2) to consider what happens if the energy release rate is suddenly changed to be larger (or smaller) than the steady state values of the fracture toughness. Realistically, the crack must accelerate (or decelerate) over a very short, but finite time interval. However, eqn (2) would unrealistically predict that with a sudden change in the energy release rate the steady state velocity would have to change instantaneously to a new steady state value. This suggests that the equation of motion must be modified to include the crack tip acceleration in order to capture non-steady or transient crack growth. Several investigators (Barenblatt and Salganik, 1963; Diaz and Lund, 1989; Liu and Marder, 1991; Marder 1991; Neimitz, 1991) have proposed specific methods to include a crack tip acceleration term into the equation of motion for the crack tip. These methods, however, are not readily applicable to general fracture configurations and loading conditions. Moreover, in some analyses (Diaz and Lund, 1989; Liu and Marder, 1991; Marder 1991), the usual near tip asymptotic fields in dynamic fracture mechanics are not preserved. In view of these difficulties and the fact that an exact derivation of an equation of motion for the crack tip may not be feasible within presently adopted approaches, the following inertia-dependent intuitive modification of eqn (2) for non-steady crack growth is proposed

$$G_d = \gamma(v) + m\dot{v} \tag{3}$$

where G_d preserves its definition (Freund, 1990) and the coefficient m is the "effective" or "attached" mass of the crack tip. [This is reminiscent of the effective mass assigned to the dislocation core (Aifantis, 1987)]. In general, the phenomenological coefficient may be a function of the crack tip velocity, specimen configuration, loading, material properties and environment, but in a first approximation it will be taken as constant. It is important to recognize that the crack tip inertia term will depend on the appropriate time and length scales of the fracture processes and, in general, its role should be assessed from transient or non-steady crack growth experiments.

In addition to the equation of motion for the crack tip, another differential equation is necessary to describe fully macroscopic stick–slip fracture under constant applied extension rate conditions. This equation can be derived by considering the compliant loading of

a cracked body. The load P is applied to the cracked body through a loading machine or device with a compliance C_m such that the total displacement Δ is given by the expression

$$\Delta = C_m P + \delta, \tag{4}$$

where δ is the load-point displacement which can be written in the form

$$\delta = C(a)P, \tag{5}$$

and $C(a)$ is the crack length-dependent compliance of the body. In general, the load-point displacement is assumed to be expressed by the sum $\delta = \delta_c + \delta_{nc}$ where δ_c is the displacement at the load-point due to the crack and δ_{nc} is the load-point displacement of the uncracked body. From eqn (5) it follows that $C = C_c + C_{nc}$, where the compliance for the cracked body is defined as $C_c = \delta_c/P$ and the compliance of the uncracked body must be determined from experiments or from an appropriate elasticity solution.

The static energy release rate G is expressed in terms of the stress intensity factor K, by the familiar formula

$$G = \frac{K^2}{\tilde{E}} = \frac{1}{2b} P^2 C', \tag{6}$$

where $\tilde{E} = E$ for plain stress and $\tilde{E} = E/(1-\nu^2)$ for plane strain, $C' = \partial C/\partial a$, b is the specimen thickness, while E and ν are the Young's modulus and Poisson's ratio, respectively.

Differentiation of eqn (6) yields:

$$\mathrm{d}G = \frac{1}{b} PC' \,\mathrm{d}P + \frac{1}{2b} P^2 C'' \,\mathrm{d}a, \tag{7}$$

where $C'' = \partial^2 C(a)/\partial a^2$. Upon introducing eqn (5) into eqn (4) and differentiating, we have

$$\mathrm{d}P = \frac{1}{C_m + C} [\mathrm{d}\Delta - PC' \,\mathrm{d}a] \tag{8}$$

which, in view of eqn (7), gives the following differential equation (after dividing by the time differential $\mathrm{d}t$) for the energy release rate

$$\dot{G} = \frac{1}{C_m + C} \left[\frac{1}{b} PC' \dot{\Delta} - \left\{ \frac{1}{b} (PC')^2 - \frac{1}{2b} P^2 C''(C_m + C) \right\} v \right]. \tag{9}$$

The stress intensity factor for common fracture test specimen geometries (e.g. double torsion, compact tension, wedge opening loaded, double cantilever beam and tapered double cantilever beam specimens) are compiled in handbooks (Murakami, 1986) and can be written in the general form

$$K = \frac{P}{b\sqrt{W}} f(a/W), \tag{10}$$

where W is a geometric parameter and $f(a/w)$ is a known function. Introducing eqn (10) into eqn (6), the energy release rate can be expressed as

$$G = \frac{P^2}{b^2 WE} f^2(a/W) \tag{11}$$

and it follows from the comparison of eqns (11) and (6) that

$$C' = \frac{2f^2(a/W)}{bWE}. \tag{12}$$

Therefore, the relevant terms in eqn (9) can be rewritten in the form

$$PC' = \frac{2Pf^2(a/W)}{bWE}, \quad P^2C'' = \frac{4P^2f(a/W)f'(a/W)}{bW^2E}, \tag{13}$$

where $f'(a/W) = \partial f(a/W)/\partial(a/W)$. [The compliance C can thus be determined by integrating eqn (12)].

Alternatively, the energy release rate G can be expressed as a function of the total displacement Δ and the crack length a, such that,

$$\dot{G} = \left(\frac{\partial G}{\partial \Delta}\right)_a \dot{\Delta} + \left(\frac{\partial G}{\partial a}\right)_\Delta v. \tag{14}$$

Comparison of eqns (9) and (14) yields

$$\left(\frac{\partial G}{\partial \Delta}\right)_a = \frac{1}{C_m + C}\frac{1}{b}PC', \tag{15a}$$

$$\left(\frac{\partial G}{\partial a}\right)_\Delta = -\frac{1}{C_m + C}\frac{1}{b}(PC')^2 + \frac{1}{2b}P^2C''. \tag{15b}$$

The terms PC' and P^2C'' in eqns (15a,b) are always positive and it follows from eqn (14) that a necessary condition for stick–slip fracture to occur for a specimen configuration under constant extension rates is the same condition as for stable crack growth to occur under a fixed displacement loading condition for a material with a fracture toughness independent of the crack growth increment Δa [i.e. $\partial\gamma/\partial(\Delta a) = 0$]; (Kanninen and Popelar, 1985), i.e.

$$\left(\frac{\partial G}{\partial a}\right)_\Delta < 0 \tag{16}$$

or equivalently

$$\frac{1}{b}(PC')^2 - \frac{1}{2b}P^2C''(C_m + C) > 0. \tag{17}$$

If this condition is not satisfied then according to eqn (14) $\dot{G} > 0$ and the energy release rate G will increase continuously as the crack length increases, which means the crack tip velocity cannot be controlled after a fracture instability occurs (i.e. the crack tip continues to accelerate and a "fast" rather than a "stick–slip" fracture occurs). In addition, it follows from eqn (17) that a stiff loading machine (low C_m) may be necessary for certain specimen configurations in order to satisfy this condition. This demonstrates the frequently imposed necessity of using a stiff loading system when examining stick–slip fracture experimentally (Maugis, 1985).

For use in the numerical calculations of the next section, the expressions for the compliance, energy release rate and its differential equation are shown explicitly for the double torsion (DT) specimen which is commonly used in fracture tests of polymers. The compliance for the DT specimen under plane strain is linear in the crack length and can be written as (Murakami, 1986)

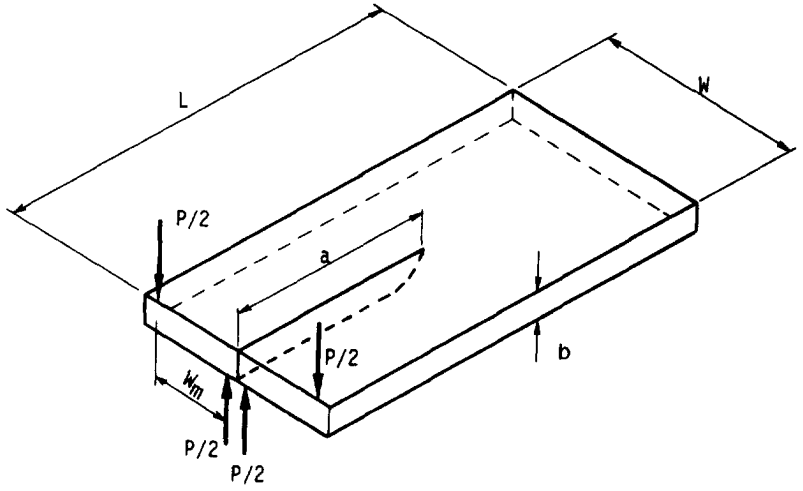

Fig. 2. Double torsion specimen and dimensions (Murakami, 1986).

$$C(a) = \frac{6(1+\nu)W_m^2 a}{Eb^3 WZ}, \tag{18}$$

where W_m and W are geometric parameters shown in Fig. 2 and Z is the thickness correction factor. Introducing eqn (18) in eqn (6) and making use of eqns (4) and (5), the energy release rate can be written in terms of the load or total displacement in the form

$$G = \frac{3(1+\nu)W_m^2 P^2}{Eb^3 b_c WZ} = \frac{Eb^3 WZ}{12b_c(1+\nu)W_m^2 a^2} \frac{\Delta^2}{\left(1+\dfrac{C_m Eb^3 WZ}{6(1+\nu)W_m^2 a}\right)^2}, \tag{19}$$

where b_c denotes the thickness at the crack tip for a side-grooved specimen. Taking the time derivative of eqn (19), the differential equation for the energy release rate may be written in the form

$$\dot{G} = \kappa(V - v), \tag{20}$$

where

$$\kappa = \frac{2G}{a\left(1+\dfrac{C_m Eb^3 WZ}{6(1+\nu)W_m^2 a}\right)}, \quad V = \sqrt{\left[\frac{Eb^3 WZ}{12b_c(1+\nu)W_m^2}\right]}\frac{\dot{\Delta}}{\sqrt{G}}. \tag{21}$$

The DT specimen is referred to as a constant K (or G) specimen because when the load is constant under stable crack growth conditions then G (or K) is constant according to eqn (19). Another feature of this specimen is that because the compliance is linear to the crack length then stable crack growth is self-similar (i.e. changes in Δ result in proportional changes in crack length). Also, it is interesting to note that the crack tip velocity can always be controlled for a constant K specimen, since eqn (17) is satisfied regardless of the loading machine compliance since $C'' = 0$.

Equation (20) provides a relationship between the constant applied extension rate $\dot{\Delta}$ and the local crack tip velocity v. However, in some fracture test configurations (e.g. peeling, tearing, wedging, scraping, etc.) the relationship between the load-point displacement and load cannot be described by eqn (4) and, thus, an alternative analysis is necessary for deriving a suitable relationship between load-point velocity (global) and crack tip velocity

(local) (Barenblatt and Salganik, 1963; Maugis and Barquins, 1987; Webb and Aifantis, 1989; Tsai and Kim, 1993).

The qualitative behavior of the crack tip oscillations can be investigated within the framework of non-linear dynamics. Thus, for a relatively small amount of crack growth ($a \approx$ constant) and for cases where the energy release rate oscillates about an average value, it is not unreasonable to approximate κ and V as constants. Then eqns (20) and (3) form an autonomous system of two first order differential equations,

$$\dot{G} = \kappa(V - v), \tag{22a}$$

$$\dot{v} = \frac{1}{m}(G - \gamma(v)), \tag{22b}$$

where $g(v)$ in eqn (1) was approximated by unity for simplicity. The qualitative behavior of the system of eqn (22a,b) is governed by the first order differential equation

$$\frac{dG}{dv} = m\kappa \frac{(V - v)}{(G - \gamma(v))}, \tag{23}$$

obtained by dividing eqn (22a) with eqn (22b). In the phase plane (G, v) the solution is a family of integral curves $G = G(v; \lambda)$ where λ is a constant and the slope of the tangents at every point of the integral curves is given by eqn (23). Furthermore, at each point of the phase plane (except at the singular points) there passes a unique integral curve (Andronov *et al.*, 1987). For eqn (23) there is only one singular point, i.e

$$v = V, \tag{24a}$$

$$G = \gamma(V), \tag{24b}$$

which corresponds to steady state cracking since eqns (24a, b) define the equilibrium state of eqns (22a, b). It follows from linearizing eqns (22a, b) that the equilibrium state is stable when $\partial\gamma(V)/\partial v > 0$ and unstable when $\partial\gamma(V)/\partial v < 0$. Furthermore, when $|\partial\gamma(V)/\partial v| > 2\sqrt{(\kappa m)}$ the singular point is a node and the integral curves approach (for stable case) or leave (for unstable case) the singular point in an periodic fashion. However, when $|\partial\gamma(V)/\partial v| < 2\sqrt{(\kappa m)}$ the singular point is a focus and the integral curves spiral towards (for stable case) or spiral away from (for unstable case) the singular point.

It can be shown that the integral curves leaving the unstable singular points when one attempts to impose a crack tip velocity V within the instable negative slope region approach a stable limit cycle (Minorsky, 1962). The limit cycle corresponds to undamped (periodic) oscillations which are commonly referred to as self-oscillations. An interesting feature is that the amplitude of these non-linear oscillations is independent of the initial conditions and depends only on the form of the system of governing equations. In other words, the non-linear oscillations depend on the non-monotonic fracture toughness–velocity and the elastic behavior of the fracture specimen and testing machine. The direction of the integral curves and limit cycle is given by eqns (22a, b) and it follows that they are in the clockwise direction. In the limiting case where the "effective" mass of the crack tip approaches zero, eqn (23) reduces to

$$dG(G - \gamma(v)) = 0. \tag{25}$$

This implies that the limit cycle is $dG = 0$ (G = const.) and $G = \gamma(v)$. The self-oscillations in this case are referred to as relaxational oscillations and this is the limit cycle usually assumed in macroscopic stick–slip fracture (Kramer and Hart, 1984; Maugis, 1985; Tsai

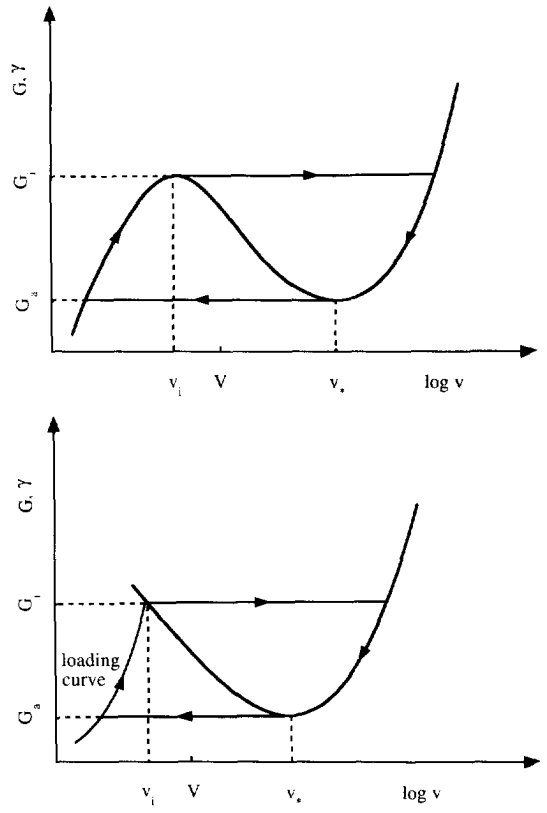

Fig. 3. Schematics of "classical" limit cycles for macroscopic stick–slip fracture.

and Kim, 1993). In Figs 3(a, b) it can be seen that the crack accelerates rapidly at $v = v_i$ and $G = G_i$ and "jumps" to the stable high velocity branch. The crack decelerates as the energy release rate decreases and "arrests" at $G = G_a$. The crack accelerates and propagates slowly on the stable low velocity branch as the energy release rate increases. Fast macroscopic crack initiation occurs when $G = G_i$ and $v = v_i$ and the process repeats itself. However, in the next section it will be shown that this "classical" relaxational limit cycle is sometimes insufficient to describe some experimental fracture observations for epoxy resins.

The relaxational limit cycles are shown schematically in Figs 3(a, b) for the two different types of non-monotonic fracture toughness–velocity curves discussed in Section 2. In Fig. 3(b) a positive slope branch called the loading curve is introduced since there is no experimentally measured stable, subcritical branch in this case. For convenience, the loading curve is treated as if it were part of the fracture toughness–velocity curve $\gamma(v)$, however, it is pointed out that the loading curve in Fig. 3(b) is not an intrinsic material property like the slow, stable branch in Fig. 3(a). In particular, the loading curve represents the non-steady, subcritical and/or "apparent" crack growth due to pre-macroscopic fracture processes, such as localized plasticity (i.e. crack tip blunting), microcracking and crazing which may occur in front of the crack tip during loading of the specimen. Since these fracture processes are, in general, time-dependent it is reasonable to assume that the loading curve would depend on the applied extension rate, specimen geometry and the loading machine compliance that influence the local crack tip opening or loading rate. The loading curve can be assumed as a steady material property if the crack tip acceleration and loading rate are low enough to enable the fracture processes ahead of the crack tip to achieve steady state during loading. In this case the loading curve and the stable, subcritical branch will coincide as shown in Fig. 3(a). In principle, the loading curve may be determined theoretically from an appropriate crack tip analysis or empirically from appropriate experimental measurements. Here, however, the loading curve is assumed to be of a power-law form

$$\gamma(v) = \gamma_0(1 + \gamma_1 v^n), \tag{26}$$

where γ_0, γ_1 and n are phenomenological coefficients, which depend on the specimen configuration, loading machine compliance, applied extension rate and material properties. This form is motivated by corresponding expressions for subcritical crack growth (Maugis, 1985) and viscoelastic cohesive zone analyses (Kanninen and Popelar, 1985). Other forms for the loading curve are also possible.

In the nearly linear case when $|\partial\gamma(V)/\partial v| < 2\sqrt{(\kappa m)}$, a perturbation analysis can be applied to eqns (22a, b). In particular, the method of multiple scales (Nayfeh, 1981) is used to determine a uniform first-order expansion of eqns (22a, b) about $v = V$ for an initial condition of $v = v_i$. This first-order expansion is given by

$$v \approx V + \sqrt{\left(\frac{-8\partial\gamma(V)/\partial v}{\partial^3_\gamma(V)/\partial v^3}\right)}\left[1-\left(1+\frac{8\partial\gamma(V)/\partial v}{\partial^3_\gamma(V)/\partial v^3(v_i-V)^2}\right)e^{\frac{(\partial\gamma(V)/\partial v)t}{m}}\right]^{-1/2}\cos\left(\sqrt{\frac{\kappa}{m}}\,t\right). \tag{27}$$

It can be seen from eqn (27) that if $v_i = V$ or $\partial\gamma(V)/\partial v = 0$ the amplitude of the limit cycle is zero, that is, no stick–slip fracture occurs and as $t \to \infty$ eqn (27) becomes

$$v \approx V + \sqrt{\left(\frac{-8\partial\gamma(V)/\partial v}{\partial^3_\gamma(V)/\partial v^3}\right)}\cos\left(\sqrt{\frac{\kappa}{m}}\,t\right), \tag{28}$$

which shows that the velocity is independent of the initial conditions for $v_i \neq V$.

4. NUMERICAL RESULTS

In this section numerical "experiments" are performed to examine further the behavior of the equations of stick–slip fracture. These equations are for a DT specimen under constant applied extension rates; however, it is not unreasonable to expect that the basic characteristics of these equations roughly apply to other fracture specimen geometries. Finally, numerical calculations are compared with stick–slip fracture measurements and observations in epoxy resins.

4.1. *Numerical experiments*

The governing equations of stick–slip fracture for a DT specimen can be rewritten in the non-dimensional form as follows

$$\frac{d\hat{a}}{dt} = \bar{\beta}\hat{v} \tag{29}$$

$$\frac{d\hat{v}}{dt} = \frac{1}{\bar{m}}(\hat{G} - \hat{\gamma}(\hat{v})) \tag{30}$$

$$\frac{d\hat{G}}{dt} = \frac{2\hat{G}}{\hat{a}+\bar{C}_m}\bar{\beta}\left[\bar{\alpha}\frac{\hat{\dot{\Delta}}}{\sqrt{\hat{G}}} - \hat{v}\right], \tag{31}$$

where it was assumed that $g(v)$ is unity and "$\hat{}$" indicates normalization with respect to a characteristic value. The non-dimensional variables are defined as

$$\hat{a} = \frac{a}{a_*}, \quad \hat{v} = \frac{v}{v_*}, \quad \hat{\dot{\Delta}} = \frac{\dot{\Delta}}{v_*}, \quad \hat{\gamma} = \frac{\gamma}{\gamma_*}, \quad \hat{G} = \frac{G}{\gamma_*}, \tag{32}$$

where a_* is the characteristic crack length taken as the initial crack length and v_* is the

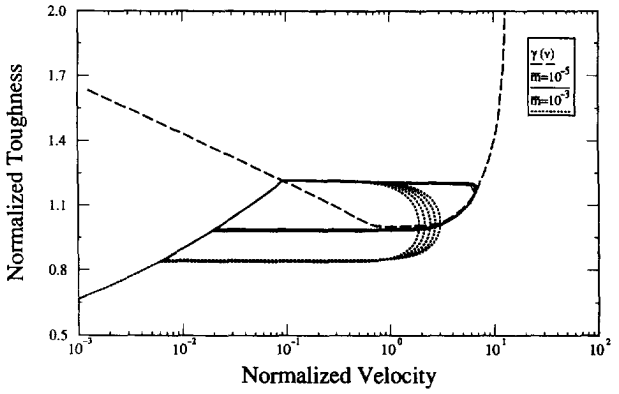

Fig. 4. The effect of crack tip inertia on limit cycles.

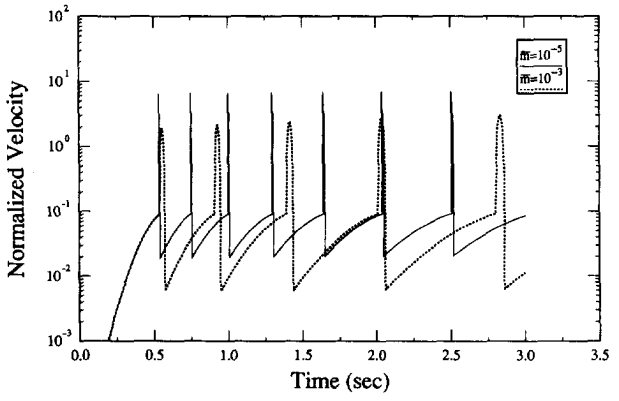

Fig. 5. Crack tip velocity profile with respect to time showing the effect of crack tip inertia.

characteristic crack tip velocity at which the fracture toughness has a local minimum γ_* [i.e. $\gamma_* = \gamma(v_*)$]. The coefficients in eqns (29)–(31) are defined as

$$\bar{\beta} = \frac{v_*}{a_*}, \quad \bar{m} = \frac{mv_*}{\gamma_*}, \quad \bar{C}_m = \frac{C_m a}{C(a)}, \quad \bar{\alpha} = \sqrt{\left(\frac{Eb^3 WZ}{12b_c(1+\nu)W_m^2\gamma_*}\right)}. \tag{33}$$

Using eqns (19) and (32) the load P for the DT specimen can be written in the form

$$P = P_*\sqrt{\hat{G}}, \quad P_* = \sqrt{\left(\frac{Eb^3 b_c WZ\gamma_*}{3(1+\nu)W_m^2}\right)}, \tag{34}$$

where $\sqrt{\hat{G}}$ can be viewed as a normalized load.

For the following numerical "experiments" the values (unless otherwise indicated) were chosen for numerical convenience to be $\bar{\beta} = 6.25\ \text{s}^{-1}$, $\bar{m} = 10^{-5}$ s, $\bar{C}_m = 0$, $\bar{\alpha} = 65.7$ and $P_* = 36.9$ N. The equation for the loading curve in non-dimensional form reads

$$\hat{\gamma}(\hat{v}) = \hat{\gamma}_0(1+\hat{\gamma}_1\hat{v}^n). \tag{35}$$

The loading curve shown in Fig. 4 is assumed to be fixed and the values of the coefficients are chosen for numerical convenience to be $\hat{\gamma}_0 = 0.1$, $\hat{\gamma}_1 = 15.9$ and $n = 0.15$. This results in the loading curve intersecting the negative slope region of the assumed non-monotonic fracture toughness curve $\hat{\gamma}(\hat{v})$ shown in Fig. 4 at $\hat{v} = \hat{v}_i = 0.093$ and $\hat{\gamma}(\hat{v}_i) = \hat{G}_i = 1.21$. The applied extension rate is chosen as $\hat{\dot{\Delta}} = 0.0025$ (unless otherwise indicated) such that the steady state crack tip velocity $\hat{V} \equiv \bar{\alpha}\hat{\dot{\Delta}}/\sqrt{\hat{G}_i} = 0.149$ is imposed with the unstable, negative slope region of $\hat{\gamma}(\hat{v})$, i.e. $\hat{v}_i < \hat{V} < 1$. The equations are integrated numerically using an Adams–Moulton routine and the behaviors of eqns (29)–(31) are plotted in Figs 4–9.

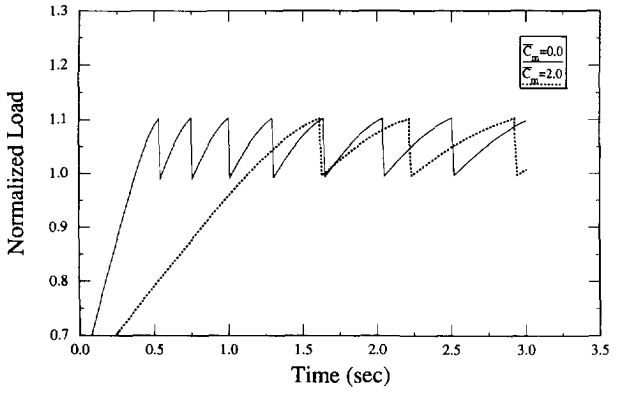

Fig. 6. Sawtooth load profile showing the influence of the loading machine compliance.

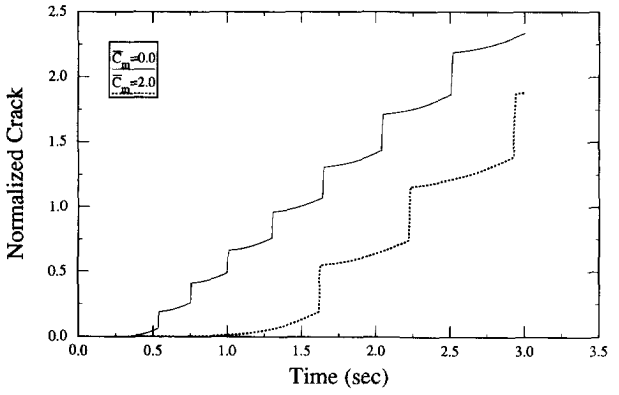

Fig. 7. Step-like crack growth showing the influence of the loading machine compliance.

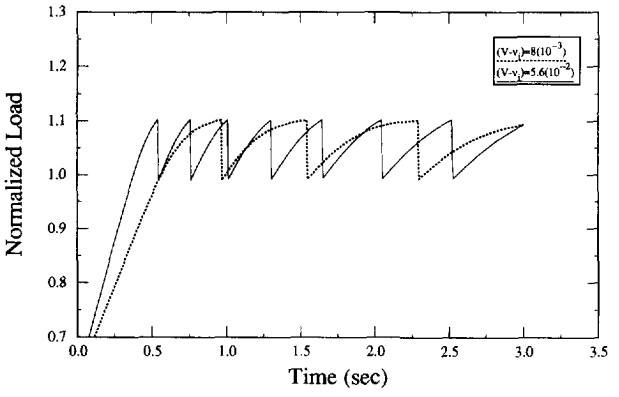

Fig. 8. Sawtooth load profile showing the effect of $(V-v_i)$.

The limit cycles in the phase plane $(\hat{G}, \hat{v})$ are plotted in Fig. 4 for two different values of the effective mass of the crack tip $\bar{m}$. For small values for $\bar{m}$ the limit cycle appears to be the relaxational type except that now there is a small but finite time interval between crack jumps. For larger values of $\bar{m}$ the "limit cycle" appears quite different from the classical limit cycle. For example, the crack tip velocity accelerates from $\hat{v} = \hat{v}_i$ to a lower velocity on the high velocity branch and decelerates from $\hat{v} = 1$ to a lower velocity on the loading curve than in the case of a small effective mass. This is illustrated in Fig. 5 where the normalized velocity $\hat{v}$ is plotted with respect to time for two different values of $\bar{m}$. In addition, this figure shows that for larger values of $\bar{m}$ the frequency of the oscillations is lower. More importantly, the energy release rate $\hat{G}$ for the non-classical limit cycle shown in Fig. 4 decreases below the local minimum fracture toughness. This result will be used

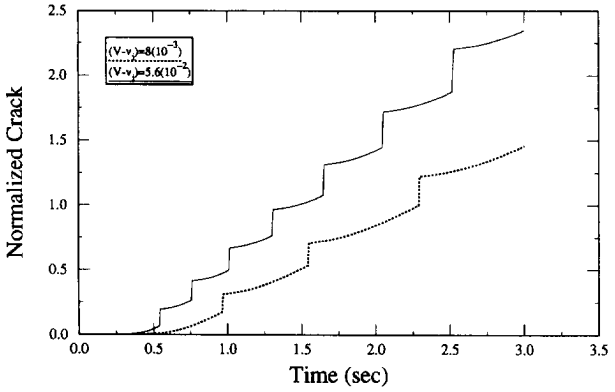

Fig. 9. Step-like crack growth showing the effect of $(V-v_i)$.

later to describe some common fracture "initiation" and "arrest" experiments on epoxy resins.

The loading machine compliance has a significant influence on the stick–slip fracture behavior. For example, the frequency of the oscillations decreases with increasing $\bar{C}_m$ as shown in Fig. 7 where the normalized load $\sqrt{\hat{G}}$ is plotted with respect to time for two different values of $\bar{C}_m$. In fact, as $\bar{C}_m$ approaches infinity the frequency of the oscillations approaches zero and stick–slip fracture will not occur. In Fig. 8 the step-like crack growth $(\Delta\hat{a} = \hat{a} - 1)$ is plotted with respect to time for two different values of $\bar{C}_m$. This figure shows how the magnitude of the "slow" crack growth increment often referred to as crack "arrest" and the magnitude of the "fast" crack growth increment increase with increasing $\bar{C}_m$. This is a direct consequence of the fact that more time is spent on the loading curve and high velocity branch, thus resulting in lower frequency oscillations. However, as shown in Fig. 7, the overall crack growth is higher in the case of a stiffer loading machine.

During the loading stage there are two competing mechanisms for which the "blunting" crack may or may not propagate rapidly as a sharp crack. Local inelastic deformation results in "small-scale" crack tip blunting, which relaxes the crack tip stress field and acts to retard the nucleation of a sharp crack from a blunted crack. At the same time damage (e.g. micro-cracks, voids, etc) accumulates in the fracture process zone ahead of the crack tip coalescing to nucleate a sharp crack from a blunted crack tip. The difference between the desired (but unobtainable) steady state velocity $\hat{V} \equiv \bar{\alpha}\dot{\hat{\Delta}}/\sqrt{\hat{G}}$ and the initiation velocity $\hat{v}_i$ for the sharp crack is a measure of the propensity for nucleation of a sharp crack from a blunted crack tip. In Fig. 8 the normalized load $\sqrt{\hat{G}}$ is plotted with respect to time for two different values of $(\hat{V}-\hat{v}_i)$. It can be seen from the figure that the commonly observed sawtooth load trace reflects the competition between the ductile and brittle mechanisms occurring during constant extension rate testing. As the difference $(\hat{V}-\hat{v}_i)$ is decreased the brittle, sharp crack tip mechanisms are retarded which results in a load trace with more curvature on the loading stage and lower frequency. This is a direct consequence of the fact that more time is spent on the loading curve (due, for example, to crack tip blunting) as shown in Fig. 9, where the normalized crack growth increment $\Delta\hat{a}$ is plotted with respect to time for two values of $(\hat{V}-\hat{v}_i)$. Also, since most of the crack growth occurs when the sharp crack is propagating rapidly on the high velocity branch, it can be seen from this figure that the overall crack growth and rate is decreased as the difference $(\hat{V}-\hat{v}_i)$ decreases.

4.2. *Comparison with experiments*

Numerical calculations are compared with the fracture experiments of Yamini and Young (1977) on epoxy resins. The applied extension rates and the corresponding upper K_i ("initiation") and lower K_a ("arrest") values of the stress intensity factor oscillations are known. The material properties and specimen dimensions defined in Fig. 2 are $W = 30$ mm, $W_m = 10.4$ mm, $Z = 0.874$, $b = 3$ mm, $b_c = 2.5$ mm, $\nu = 0.33$ and $E = 3 \times 10^3$ MPa

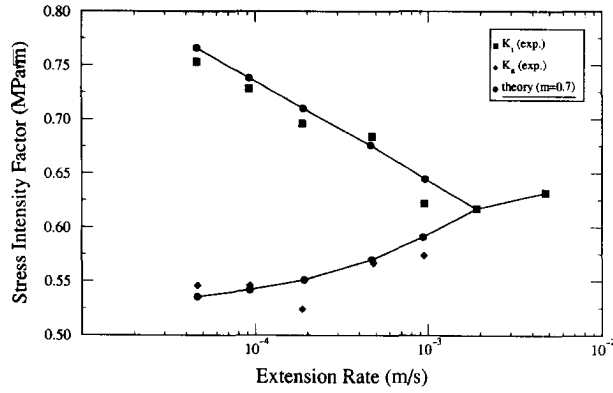

Fig. 10. Stress intensity factors (K_i, K_a) versus applied extension rate.

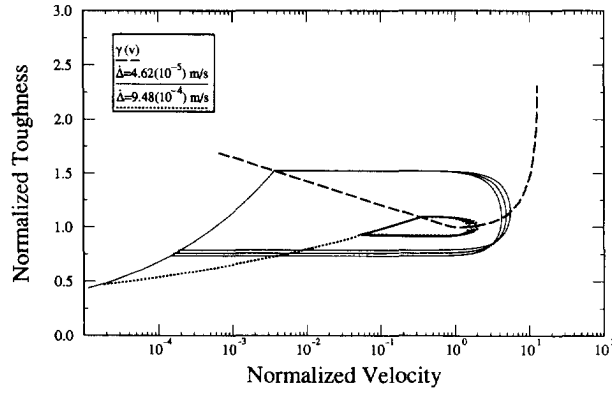

Fig. 11. Loading curves and limit cycles for two different applied extension rates.

(typical). The negative-slope region of the fracture toughness–velocity curve is approximated by replotting the experimental data shown in Fig. 10 as $G_i(V) = K_i^2/\tilde{E}$ where V for the DT specimen is given by eqn (21) for $G = G_i$. The actual negative slope region of the fracture toughness–velocity curve is defined as (G_i, v_i) and is determined by the equation for the loading curve $G_i = \gamma(v_i) = \gamma_0(1+\gamma_1 v_i^n)$ where $v_i < V$. The parameters (γ_0, γ_1, n) in the loading curve equation were chosen to match the appropriate load versus time measurements for various applied extension rates. Figure 12 shows two such loading curves for two different applied extension rates.

Equations (29)–(31) are numerically integrated for given applied extension rates and the value of the effective mass of the crack tip is chosen to produce the appropriate limit cycles shown in Fig. 12 for the construction of the theoretical K_i (or G_i) and K_a (or G_a) versus applied extension rate curves shown in Fig. 10. It can be seen in Fig. 10 that the loading curve concept successfully describes the experimentally observed decrease of K_i with increasing applied extension rates and the transition to stable crack growth at applied extension rates above $\dot{\Delta} = 1.9 \times 10^{-3}$ m s^{-1}. In addition, this figure shows the necessity of including the crack tip inertia term in the equation of motion since a classical stick–slip fracture limit cycle ($m = 0$) would predict $K_a = K_* = \sqrt{\tilde{E}\gamma_*} = 0.62$ MPa m$^{1/2}$. It can be seen that the theory compares well with the experiments for $m = 0.7$ Pa s where K_a is less than K_* and increases with increasing applied extension rates until $K_a = K_*$ at the transition to stable crack growth.

The results in Fig. 10 are not sensitive to the shape of the high velocity branch shown in Fig. 11. The shape of the high velocity branch, however, does provide an upper limit on the crack tip velocity which in turn affects the magnitude of the crack growth increments. Since the complete high velocity branch was not measured in the experiments it was chosen so that the sizes of the crack growth increments were comparable with those observed

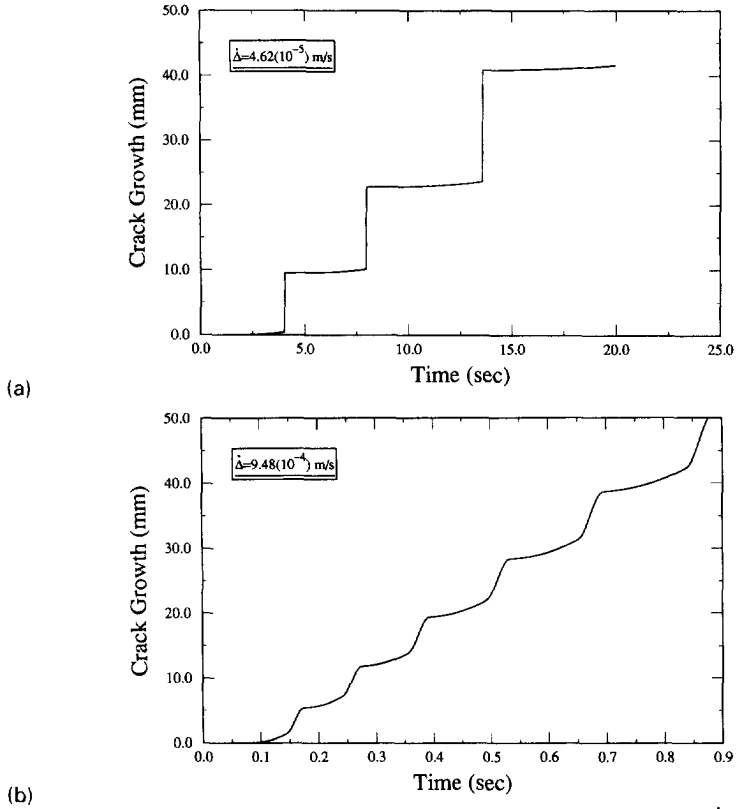

Fig. 12. Step-like crack growth for two different applied extension rates (a) for $\dot{\Delta} = 4.62 \times 10^{-5}$ m s^{-1} and (b) for $\dot{\Delta} = 9.48 \times 10^{-4}$ m s^{-1}.

experimentally. The crack growth with respect to time is plotted in Figs 12(a, b) for two different applied extension rates. These figures show that the crack growth increments are larger and the frequency of the oscillations are much lower for lower applied extension rates. The crack growth increments for the lower applied extension rate are 10–17 mm and for the higher applied extension rate are 4–10 mm. These estimates correlate well with experiments (Young and Beaumont, 1976). The shape of the loading curve influences the crack growth behavior and in the case of high applied extension rates the step-like crack growth is more rounded. Figures 12(a, b) compare well with the two types of crack growth identified by Leevers (1986).

Acknowledgements—The support of NSF under MSS-9310476 grant and AFOSR under grant AFOSR-910221 is acknowledged. The support of CEC under contract No. ERB CHBGCT 920041 is also gratefully acknowledged.

REFERENCES

Aifantis, E. C. (1987). The physics of plastic deformation. *Int. J. Plasticity* **3,** 211–247.

Aifantis, E. C. (1990). Nonlinearity and self-organization in plasticity and fracture. In *Patterns, Defects and Material Instabilities*, NATO ASI Series E-Vol. 183 (Edited by D. Walgraef and N.M. Ghoniem), pp. 221–239. Kluwer Academic, Dordrecht.

Aifantis, E. C. (1991). A proposal for a new understanding of the crack tip : a nonlinear approach. In *Constitutive Laws for Engineering Materials—Theory and Applications* (Edited by C. S. Desai, E. Krempl, G. Frantziskonis and H. Saadatmanesh), pp. 313–315. ASME Press, New York.

Aifantis, E. C. (1992). On the gradient approach to deformation patterning and fracture. *Solid St. Phenomena.* **23, 24,** 355–368.

Andronov, A. A., Vitt, A. A. and Khaiken, S. E. (1987). *Theory of Oscillators.* Dover, New York.

Atkins, A.G., Lee, C. S. and Caddell, R. M. (1975). Time–temperature dependent fracture toughness of PMMA part 2. *J. Mater. Sci.* **10,** 1394–1404.

Aubrey, D. W. (1978). Viscoelastic basis of peel adhesion. In *Adhesion* 3 (Edited by K.W. Allen), pp. 191–205. Applied Science, London.

Aubrey, D. W. and Sherriff, M. (1980). Peel adhesion and viscoelasticity of rubber–resin blends. *J. Polym. Sci.* **18,** 2597–2608.
Aubrey, D. W., Welding, G. N. and Wong, T. (1969). Failure mechanisms in peeling in pressure-sensitive adhesive tape. *J. Appl. Polym. Sci.* **13,** 2193–2207.
Barenblatt, G. I. and Salganik, R. L. (1963). On the wedging of brittle bodies. Self-oscillations during wedging. *J. Appl. Math. Mech.* **27,** 656–673.
Broutman, L. J. and Kobayashi, T. (1972). Dynamic crack propagation studies in polymers. In *Dynamic Crack Propagation* (Edited by G.C. Sih), pp. 215–225. Noordhoff, Leyden.
Carlsson, J., Dahlberg, L. and Nilsson, F. (1972). Experimental studies of the unstable phase of crack propagation in metals and polymers. In *Dynamic Crack Propagation* (Edited by G. C. Sih), pp. 165–181. Noordhoff, Leyden.
Diaz, M. and Lund, F. (1989). The inertia of a crack near a dislocation. *Phil. Mag. A* **60,** 139–145.
Fineberg, J., Gross, S. P., Marder, M. and Swinney, H. L. (1991). Instability in dynamic fracture. *Phys. Rev. Lett* **67,** 457–460.
Fineberg, J., Gross, S. P., Marder, M. and Swinney, H. L. (1992). Instability in the propagation of fast cracks. *Phys. Rev. B* **45,** 5146–5154.
Freund, L. B. (1990). *Dynamic Fracture Mechanics*. Cambridge University Press, New York.
Freund, L. B. and Hutchinson, J. W. (1985). High strain-rate crack growth in rate-dependent plastic solids. *J. Mech. Phys. Solids* **33,** 169–191.
Freund, L. B., Hutchinson, J. W. and Lam, P. S. (1986). Analysis of high-strain-rate elastic–plastic crack growth. *Engng Fracture Mech.* **23,** 119–129.
Freund, L. B. and Lee, Y. J. (1990). Observations on high strain rate crack growth based on a strip yield model. *Int. J. Fracture* **42,** 261–276.
Freund, L. B. and Rosakis, A. J. (1992). The structure of the near-tip field during transient elastodynamic crack growth. *J. Mech. Phys. Solids* **40,** 699–719.
Gardon, J. L. (1963). Peel adhesion. I. Some phenomenological aspects of the test. *J. Appl. Polym. Sci.* **7,** 625–641.
Green, A. K. and Pratt, P. L. (1974). Measurement of the dynamic fracture toughness of polymethylmethacrylate by high-speed photography. *Engng Fracture Mech.* **6,** 71–80.
Greensmith, H. W. and Thomas, A. G. (1955). Rupture of rubber. III. Determination of tear properties. *J. Polym. Sci.* **18,** 189–200.
Hakeem, M. I. and Phillips, M. G. (1979). Unstable crack propagation—a fractographic study using PMMA in liquid environments. *J. Mater. Sci.* **14,** 2901–2905.
Hart, E. W. (1980). A theory for stable crack extension rates in ductile materials. *Int. J. Solids Structures* **16,** 807–823.
Hart, E. W. (1983). Stable crack extension rates in ductile materials: characterization by a local stress-intensity factor. In *Elastic–Plastic Fracture: Second Symposium, Volume I—Inelastic Crack Analysis*, ASTM STP 803 (Edited by C. F. Shih and J. P. Gudas), pp. I-521–I-531. American Society for Testing and Materials.
Hui, C. Y. (1983). Steady-state crack growth in elastic power-law creeping materials. In *Elastic–Plastic Fracture: Second Symposium, Volume I—Inelastic Crack Analysis*, ASTM STP 803 (Edited by C. F. Shih and J. P. Gudas), pp. I-573–I-593. American Society for Testing and Materials.
Hui, C. Y. and Riedel, H. (1981). The asymptotic stress and strain field near the tip of a growing crack under creep conditions. *Int. J. Fracture* **17,** 409–425.
Irwin, G. R. (1964). Structural aspects of brittle fracture. *Appl. Mater. Res.* **3,** 65–81.
Irwin, G. R. and Paris, P. C. (1971). Fundamental aspects of crack growth and fracture. In *Fracture* (Edited by H. Liebowitz), Vol. 3, pp. 1–46. Academic Press, New York.
Isherwood, D. P. and Williams, J. G. (1978). Some observations on the tearing of ductile materials. *Engng Fracture Mech.* **10,** 887–895.
Johnson, F. A. and Radon, J. C. (1972). Molecular kinetics and the fracture of PMMA. *Engng Fracture Mech.* **4,** 555–576.
Kanninen, M. F. and Popelar, C. H. (1985). *Advanced Fracture Mechanics*. Oxford University Press, New York.
Kim, K.-S. and Kim, J. (1988). Elasto-plastic analysis of the peel test for thin film adhesion. *J. Engng Mater. Tech.* **110,** 266–273.
Kinloch, A. J. and Williams, J. G. (1980). Crack blunting mechanisms in polymers. *J. Mater. Sci.* **15,** 987–996.
Kinloch, A. J. and Yuen, M. L. (1989). The mechanical behaviour of polyimide–copper laminates part 1: locus of failure studies. *J. Mater. Sci.* **24,** 2183–2190.
Kinloch, A. J. and Yuen, M. L. (1989). The mechanical behaviour of polyimide/copper laminates part 2: peel energy measurements. *J. Adhesion* **30,** 151–170.
Kobayashi, T. and Dally, J. W. (1977). Relation between crack velocity and the stress intensity factor in birefringent polymers. In *Fast Fracture and Crack Arrest* ASTM STP 627 (Edited by G.T. Hahn and M.F. Kanninen), pp. 257–273. American Society for Testing and Materials.
Kramer, E. J. and Hart, E. W. (1984). Theory of slow, steady state crack growth in polymer glasses. *Polymer* **25,** 1667–1678.
Leevers, P. S. (1986). Crack front shape effects on propagation stability in thermosetting polyesters. *Theor. App. Fracture Mech.* **6,** 45–55.
Liu, X. and Marder, M. (1991). The energy of a steady-state crack in a strip. *J. Mech. Phys. Solids* **39,** 947–961.
Marder, M. (1991). New dynamical equations for cracks. *Phys. Rev. Lett.* **66,** 2484–2487.
Mataga, P. A., Freund, L. B. and Hutchinson, J. W. (1987). Crack tip plasticity in dynamic fracture. *J. Phys. Chem. Solids* **48,** 985–1005.
Maugis, D. (1985). Review: subcritical crack growth, surface energy, fracture toughness, stick–slip and embrittlement. *J. Mater. Sci.* **20,** 3041–3073.
Maugis, D. and Barquins, M. (1987). Stick–slip and peeling of adhesive tapes. In *Adhesion* (Edited by K. W. Allen), pp. 205–222. Applied Science, London.
Minorsky, N. (1962). *Nonlinear Oscillations*. Van Nostrand, Princeton.
Murakami, Y. (1986). *Stress Intensity Factors Handbook*. Pergamon Press, Elmsford, New York.

Nayfeh, A. H. (1981). *Introduction to Perturbation Techniques*. John Wiley, New York.
Neimitz, A. (1991). Analysis of the crack motion with varying velocity according to the Dugdale–Panasyuk model. *Engng Fracture Mech.* **39,** 329–338.
Phillips, D. C., Scott, J. M. and Jones, M. (1978). Crack propagation in an amine-cured epoxide resin. *J. Mater. Sci.* **13,** 311–322.
Popelar, C. H. (1990). A viscoplastic analysis for predicting the dynamic fracture toughness of A533B steel. *Int. J. Fracture* **46,** 185–205.
Ravi-Chandar, K. and Balzano, M. (1988). On the mechanics and mechanisms of crack growth in polymeric materials. *Engng Fracture Mech.* **30,** 713–727.
Riedel, H. (1990). Creep crack growth under small-scale creep conditions. *Int. J. Fracture* **42,** 173–188.
Ripling, E. J., Mostovoy, S. and Patrick, R. L. (1964). Application of fracture mechanics to adhesive joints. In *Adhesion* ASTM STP 360, pp. 5–19. American Society for Testing and Materials.
Scott, J. M., Wells, G. M. and Phillips, D. C. (1980). Low temperature crack propagation in epoxide resin. *J. Mater. Sci.* **15,** 1436–1448.
Selby, K. and Miller, L. E. (1975). Fracture toughness and mechanical behavior of an epoxy resin. *J. Mater. Sci.* **10,** 12–24.
Takahashi, K. (1987). Dynamic fracture instability in glassy polymers as studied by ultrasonic fractography. *Polym. Engng Sci.* **27,** 25–32.
Tsai, K.-H. and Kim, K.-S. (1993). Stick–slip in the thin film peel test-I. The 90° peel test. *Int. J. Solids Structures* **30,** 1789–1806.
Webb, T. W. and Aifantis, E. C. (1989). Stick–slip peeling. ASME Winter Annual Meeting, San Francisco, California, No. 89-WA/EEP-47.
Williams, J. G. (1972). Visco-elastic and thermal effects of crack growth in PMMA. *Int. J. Fracture Mech.* **8,** 393–401.
Williams, J. G. (1984). *Fracture Mechanics of Polymers*. Ellis Horwood, Chichester, UK.
Williams, J. G., Radon, J. C. and Turner, C. E. (1968). Designing against fracture in brittle plastics. *Polym. Engng Sci.* **8,** 130–141.
Yamini, S. and Young, R. J. (1977). Stability of crack propagation in epoxy resins. *Polymer* **18,** 1075–1080.
Yamini, S. and Young, R. J. (1979). Crack propagation in and fractography of epoxy resins. *J. Mater. Sci.* **14,** 1609–1618.
Young, R.J. and Beaumont, P. W. R. (1976). Crack propagation and arrest in epoxy resins. *J. Mater. Sci. Lett.* **11,** 776–779.